Heat-flux induced changes to multicrystalline D_2 surfaces

G. W. Collins, T. P. Bernat, E. R. Mapoles, and B. J. Kozioziemski
Lawrence Livermore National Laboratory, Livermore, California 94551

C. Duriez
CEA, Centre d'Etudes de Limeil-Valenton 94195 Villeneuve-St-Georges-Cedex, France
(Received 8 February 2001; published 30 April 2001)

Phase-shifting interferometry reveals that a heat flux normal to the gas-solid interface reduces the surface roughness of thick (10–300 μm) multicrystalline D_2 films. The initial roughness, caused by misaligned crystals and grain boundaries produced during the initial random nucleation and rapid crystal growth used in the experiment decreases with increasing heat flux. A simple energy minimization model quantitatively explains the functional relationship between surface roughness and heat flux.

DOI: 10.1103/PhysRevB.63.195416 PACS number(s): 68.35.Ct, 81.10.Bk, 81.10.Aj

Very smooth and uniform 50–300 μm-thick deuterium-tritium (D-T) layers on the interiors of 1–3 mm-diameter spherical capsules are required for ignitable inertial confinement fusion (ICF) targets for the National Ignition Facility.[1,2] Such D-T layers develop through a natural redistribution process driven by bulk-solid heating from tritium beta decay.[3–5] This process typically results in a multicrystalline D-T layer with the average solid-gas interface conforming to an isotherm of the spherical container. These thick multicrystalline films grown from the liquid or vapor are not perfectly smooth. The surface structure is a function of the distribution of crystallite sizes, orientations, etc., determined largely by the initial nucleation and growth.[6] Herring,[7,8] and Mullins[9] set the groundwork for understanding this surface structure. Typically, when a smooth or flat surface finish is required, slow, material-dependent techniques, such as epitaxial growth, are used. These techniques are not available for smoothing ICF fuel layers. A search for alternative methods motivated the present work. We show that a heat flux applied normal to the gas-solid interface smoothes 10–300 μm-thick solid D_2 surfaces. This result may have more general application for controlling multicrystalline surface morphologies. An extensive literature exists on the theory of crystal shapes, but it does not apply to the present work. We therefore present a simple energy-minimization model of the effects of a thermal gradient on multicrystalline surface roughness, which quantitatively fits our data with reasonable choices of crystal parameters.

The D_2 films were grown from the vapor phase by cooling through the triple-point temperature of 18.73 K in a cell schematically shown in Fig. 1. The top and bottom plates are MgF_2-coated sapphire. The bottom plate is at temperature T_1 and serves as the substrate for growing D_2 films. The top plate is at temperature T_2 and allows optical access to the D_2 films. Raising T_2 several degrees above T_1 produces a heat flux F at the gas-solid surface. For films that are thin compared to $x=3.84$ mm, the distance between the top and bottom plates, $F=\kappa_v(T_2-T_1)/x$, where κ_v is the vapor thermal conductivity for the average temperature between the plates. A fill tube (not shown) enables us to monitor the D_2 vapor pressure in the cell. Calibrated germanium resistance thermometers measure both T_1 and T_2. Except when noted, the temperature stability was better than 0.005 K for a 2 h period.

Surface roughness is determined from both surface-reflection phase maps and optical-path-depth phase maps. The phase maps are measured by placing the sample in one arm of a phase-shifting Michelson interferometer operating at 589 nm with a 30 nm bandwidth. A 3× objective images a 2.98×2.57 mm^2 area of D_2. Surface-reflection phase maps, where the D_2 solid-gas surface forms one of the ''mirrors'' of the interferometer, are the most sensitive to surface structure but are limited to surfaces smoother than 1 μm rms. Phase maps can be measured to $\lambda/50$ giving a sensitivity to height variations of 10 nm. For rougher surfaces, the complex and tightly spaced fringes cannot be reduced to a surface structure. For these rough layers the solid D_2-MgF_2 interface is used as the interferometer sample-arm mirror and the optical-path-depth phase map characterizes the D_2 layer uniformity. The MgF_2 surface roughness (<1 nm rms) is much smaller than the D_2 surface roughness (>100 nm rms), so the measured phase is modulated predominantly by the spatial variation of the D_2 layer thickness. Since the refractive index of D_2 is 1.16, optical-path-depth phase maps can

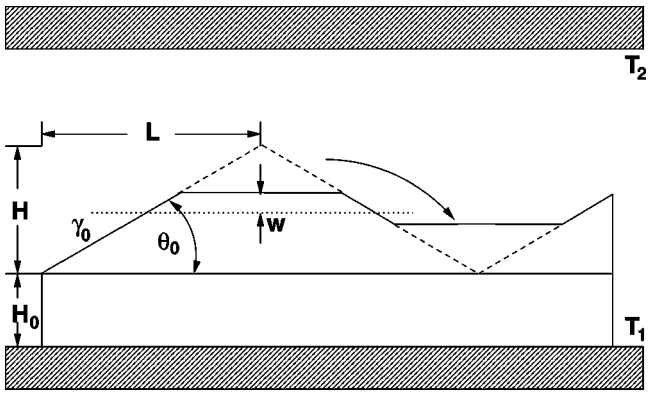

FIG. 1. Sketch of the sample arrangement. Solid deuterium films are grown on the cold substrate at temperature T_1. The top plate, at temperature $T_2>T_1$, is used to generate a heat flux through the D_2 layer to reduce surface roughness. The layer thickness H_0 is not a factor in the heat flux model.

measure roughness rms values up to $\sigma = 6\ \mu$m and the height-change sensitivity is 60 nm. The measured σ from both techniques is the same to within 20%, for surfaces with $1 > \sigma > 0.4\ \mu$m, suggesting that there is little density nonuniformity in the D_2 films and the solid D_2-MgF_2 interface is smooth in comparison to the D_2 solid-gas interface. We measure the film thicknesses by increasing the light bandwidth to $\approx$500 nm and measuring the distance the sample must be moved to bring a single ''white-light'' fringe from the solid D_2-MgF_2 interface to the D_2 gas-solid interface. The accuracy is 3 μm.

If all crystal planes had the same specific surface energy and there were no effects due to grain boundaries, the surface of the solid D_2 would lie along isotherms of the sample cell. To determine this ideal surface profile, we modeled the isotherms using the finite-element code COSMOS. The model indicates a small quadratic component of the isotherms ($h \approx ax^2 + by^2$) which results in a maximum deviation of 5% in layer thickness for a 100-μm-thick D_2 layer. All higher-order terms in the isotherms ($h \approx ax^n + by^m, n, m > 2$) are several orders of magnitude smaller than the quadratic. σ that we report is the standard deviation of surface height values after subtracting a second-order fit to the surface.

Figure 2(a) shows $\sigma(t)$ versus time for several D_2 layers nominally 100 μm thick. The layers were grown by cooling the sample cell at the rate of 0.002 K/s to the final temperature. Time zero is when the final temperature is reached, after which the layer thickness was constant to within 15%. The dark squares, triangles, circles, and diamonds had $T_1 = 18.6$ K, but different values for T_2 and thus F. The open circles had $T_1 = 17.48$ K. For the data in Fig. 2(a), F was constant throughout each run, including the layer-growth phase. The rms surface roughness decays exponentially, $\sigma(t) = \sigma_0 \exp(-t/\tau) + \sigma_{ss}$. The time constants τ, and asymptotic steady-state limits σ_{ss} decrease with increasing heat flux. F can also be increased after initial layer formation to reach lower values of σ_{ss}. This smoothing process is not simply an anneal. It does not occur if there is no heat flux even though the D_2 is just below the triple point, as shown by the constant roughness for the dark squares in Fig. 2(a).

To estimate surface-roughness time dependence in the presence of a heat flux, we consider a simple one-dimensional model. A thick film of solid D_2, just after freezing, contains thickness variations due to the anisotropic crystal growth. At any point on the surface, the temperature can be obtained from Laplace's equation using $\kappa_s (dT/dy)|_{y=h} = F + (dn/dt) L_s$ as a boundary condition, where κ_s is the solid thermal conductivity, dn/dt is the molecular flux at the surface, h is the layer thickness, and L_s is the latent heat. The net molecular flux at the surface is obtained from the difference between the incident flux, which is proportional to the average vapor pressure, and the exiting flux, which is proportional to the solid vapor pressure at the surface temperature. In this simple model, initial height variations decay away with a single exponential as observed, with the time constant,

$$\tau = \frac{\kappa_s \rho_s}{F} \left(\frac{\sqrt{2\pi m k_b \overline{T}}}{\left. \frac{\partial P_y}{\partial T} \right|_{\overline{T}}} + \frac{L_s h}{2\kappa_s} \right), \qquad (1)$$

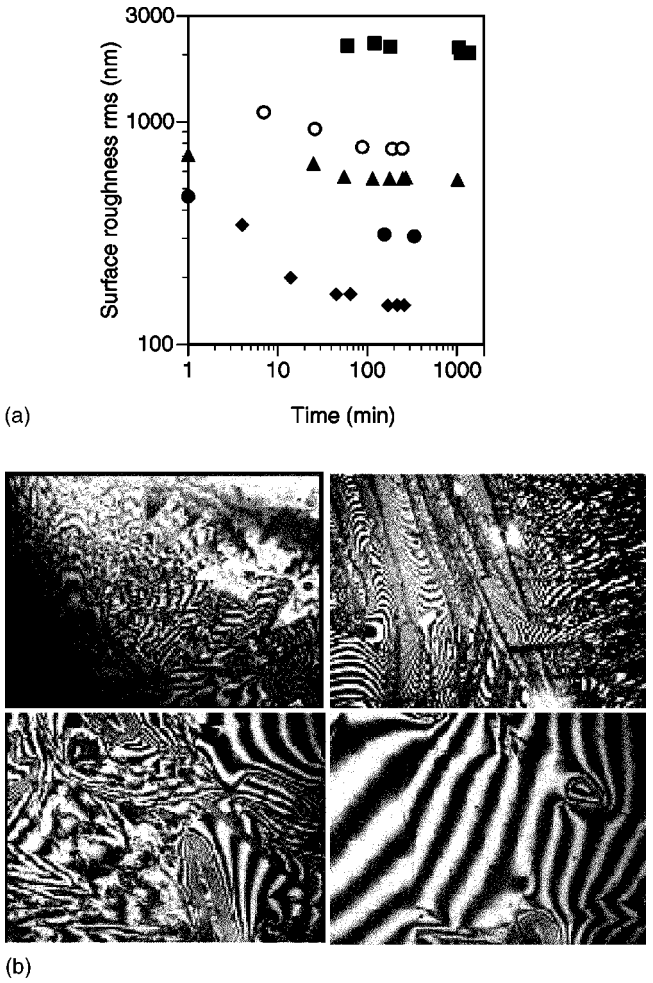

FIG. 2. (a) Surface roughness rms vs time for 100-μm-thick D_2 films grown by cooling from the liquid at 0.002 K/sec to the final set-point temperature T_1. For the dark squares $T_1 = 18.67$ K, $F = 0.23$ mW/cm^2; dark triangles $T_1 = 18.55$ K, $F = 0.85$ mW/cm^2; dark circles $T_1 = 18.5$ K, $F = 1.6$ mW/cm^2; dark diamonds $T_1 = 18.54$ K, $F = 3.6$ mW/cm^2; and open circles $T_1 = 17.49$ K, $F = 1.6$ mW/cm^2. (b) White-light interferograms of D_2 layers corresponding to data points in (a). Top left: crystals growing during cool-down through the triple point. Top right: dark squares, 1230 min after freezing. Lower left and right: dark diamonds at 3 and 175 min, respectively. The vertical field is 2 mm. The mismatched crystal boundaries are highlighted by fringe density discontinuities.

where ρ_s is the molecular density of the solid, m is the mass of D_2, k_b is the Boltzmann's constant, $\overline{T}$ is the average surface temperature, $\partial P_y/\partial T|_{\overline{T}}$ is the derivative of the vapor pressure with respect to temperature evaluated at $\overline{T}$, and h is the final layer thickness. The vapor-pressure-dependent term makes little contribution except at low temperatures. This simple model predicts the correct functional dependence for the roughness, but it predicts a time constant that is a factor of about 4 smaller than the measured value. This agreement is surprisingly good given that the redistribution process is far from 1D and the anisotropic nature of the surface energy, which produces the initial surface nonuniformity, is ignored.

Figure 2(b) shows surface reflection interferograms to reveal the multicrystalline nature of the data in Fig. 2(a). The

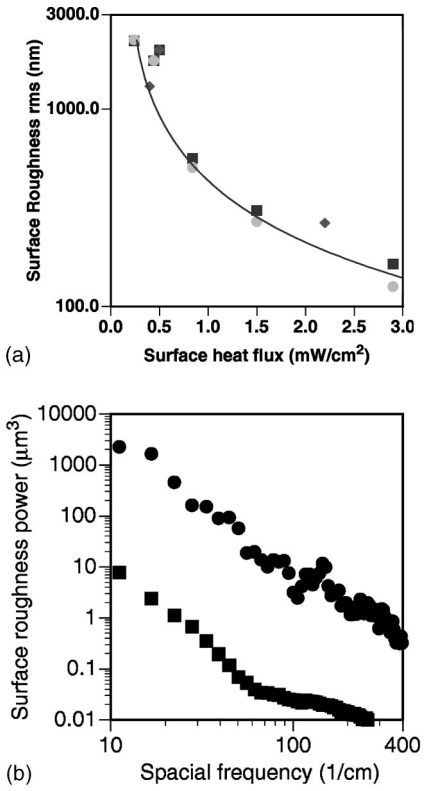

FIG. 3. (a) Surface roughness rms vs applied heat flux through the 100-μm-thick D_2 layer. The squares were measured with optical-path-depth phase maps at $T=18.6$ K. The circles and diamonds were measured with surface reflection phase maps at $T=18.6$ and 18 K, respectively. The solid line is from Eq. (4) with the parameters stated in the text. (b) Surface roughness power spectra for the same layers shown in (a); circles, $F=0.5$ mW/cm^2 and squares, $F=1.6$ mW/cm^2.

close spacing and abrupt orientational changes of the fringes in the upper panels shows the multicrystalline surface. The initial surface roughness varies from run to run due to random crystal nucleation and growth, and are not correlated with the growing heat flux. At larger heat fluxes, with time crystal facets become smoothly curved, the height jumps between different crystals decrease, and cusps at grain boundaries are removed.

Figure 3(a) shows σ_{ss} versus heat flux for 100-μm-thick solid D_2 films at 18.0 and 18.6 K. As mentioned above, σ_{ss} from both surface reflection and optical-path-depth measurements have nearly the same value, suggesting that most of the large optical-path nonuniformities are due to surface roughness at the D_2 solid-gas interface. Figure 3(b) shows the roughness power spectra $P(f)$ for two samples used in Fig. 3(a). These and similar spectra show a significant decrease in roughness amplitude for all the spatial frequencies measured, upon increasing F from 0.5 to 1.6 mW/cm^2. Above 1.6 mW/cm^2, we do not typically observe a further decrease in the high-frequency amplitudes ($f>20\,\mathrm{mm}^{-1}$). The low-frequency [$10<f(\mathrm{mm}^{-1})<0.3$] amplitudes, which dominate σ_{ss} in Fig. 3(a), continue to decrease with increasing F to 3.6 mW/cm^2.

The observed reduction in σ_{ss} in the presence of the applied heat flux occurs because higher surface perturbations have a higher temperature and thus vapor pressure relative to lower points. This causes a sublimation and recondensation from the higher to the lower points, resulting in a smoother surface. The process is accompanied by the exposure of many high-index crystal planes, which generally have higher specific surface energies. The final surface configuration, and thus roughness, results from a competition between the sublimation process decreasing the bulk thermal energy in the presence of a flux-driven thermal gradient, and the increasing surface energy from the high-index surface planes. An energy-minimization model estimates the heat flux dependence of the surface height $h(\alpha,\mathbf{r})$, subject to the constant volume constraint and applicable boundary conditions. The total energy, neglecting grain boundaries, is

$$E_T=\int_S \gamma(h')\sqrt{1+h'^2}\,dA+\int\int_V e(\mathbf{x})\,dV, \tag{2}$$

where $\gamma(h')$ is the orientation-dependent surface energy, and $e(\mathbf{x})$ is the thermal energy density at $\mathbf{x}=(x_1,x_2,x_3)$. The first integral is the total surface energy, which is the commonly used starting point for crystal shape calculations, and leads to the well-known Wulff theorem.[10] The thermal energy term is new and unique to our experiments.

Most of the relevant physics associated with this energy minimization procedure is revealed with the simply parametrized model surface of Fig. 1, without performing the full variational calculation. While actual surfaces have crystals of various lengths and tilts and with different crystal planes exposed, our model simplifies this initial surface. The morphology is assumed to be two-dimensional for ease of calculation, i.e., the initial surface is assumed to be a corrugation of tilted crystal planes, with common tilt angles θ_0 and common width L. The initial crystal planes are assumed to be low-index, consistent with the lowest-energy equilibrium configuration, and each is given the same specific surface energy γ_0.

Moving small triangles from the peaks to the troughs of the crystal corrugations reduces the overall thermal energy, but creates vicinal surfaces with higher surface energies, $\gamma(\theta)$. We choose $\gamma(\theta)=\gamma_0+\gamma_1|\theta-\theta_0|$ to model the energy of the vicinal planes, a form consistent with the literature,[11] where θ is the slope of the vicinal plane, and γ_1 is proportional to the step energy. These vicinal surfaces are at heights w above and below the average height. Assuming one-dimensional heat transfer in the y direction, the energy density is $e(x,y)=e_0+cFy/2\kappa_s$, where c is the volumetric specific heat of the hydrogen ice and e_0 is the reference thermal energy density when no thermal gradient exists. The value of w that minimizes the total energy as calculated from Eq. (2) is

$$w_{\min}=\frac{H}{4}\left[1-\left(1-\frac{8\Delta\gamma}{kH^2}\right)^{1/2}\right], \tag{3}$$

with $\Delta\gamma=\gamma_0[1-\cos(\theta_0)^{-1}]+\gamma_1|\theta|$ and $k=cF/2\kappa_s$. The rms roughness of the corrugated surface is

$$\sigma=w(1-4w/3H)^{1/2}. \tag{4}$$

The roughness as a function of heat flux from Eqs. (3) and (4) is plotted in Fig. 3(a) for $L=125\,\mu$m, $\theta=0.10$, $\gamma_0=6$ ergs/cm^2, $\gamma_1=0.8$ ergs/cm^2, and $c=5.5\times10^5$ ergs/(cm K) and compares well with the experimental data. Other combinations of these parameters produce acceptable fits, but H and L should match experimentally observed crystals and initial roughness, and a lower limit exists for γ_0 from the stability of facets at the triple-point temperature.[12]

Two conditions are imposed on this model. The first is that $\Delta\gamma(\theta)$ must be positive, otherwise the surface is not in equilibrium before the heat flux is applied. The second condition is that $w_{\min}$ must be real, or $F>16\kappa_s\Delta\gamma(\theta)/(cH^2)$. This sets the threshold value of the heat flux required for the decrease in thermal energy to exceed the increase in surface energy. With these two conditions, the model predicts that the small-length-scale crystals ($<75\ \mu$m) are more difficult to smooth than longer crystals. Each of the surfaces of Fig. 2(b) actually consists of an ensemble of crystals with different initial slopes and lengths, and also several different exposed crystal planes. These differing initial surfaces may account for much of the scatter of the data about the model line. Small isolated defects in an otherwise smoothed surface, such as shown in Fig. 2(b) may persist because F is below the threshold value. The defect about a third of the way down the right side of that image has $L\approx50\,\mu$m and, from the interference fringes, $H=1.2\,\mu$m. The 3.6 mW/cm^2 heat flux is smaller than the 10 mW/cm^2 predicted by the model as necessary to smooth the bump.

The low-temperature ($T=17.49$ K) data set in Fig. 2 has a larger surface roughness than the 18.5 K data. Indeed, low-temperature surfaces typically contained more facets and were harder to smooth with heat flux. The model calculation contains a temperature dependence through the heat capacity which increases as T^3, and surface energies whose temperature dependence we do not know. However, the scatter in the low-temperature data was too large to determine a clear dependence of σ on T. Finally, we also found that the multicrystalline surface roughness increases as the average layer thickness increases from 10 to 300 μm, with the increase in σ versus thickness decreasing with increasing heat flux. No increase in surface roughness versus layer thickness is predicted with our model.

The authors acknowledge the contributions of Walter Unites who was instrumental in constructing the apparatus, and in collecting data. This work was performed under the auspices of the U.S. Department of Energy by the Lawrence Livermore National Laboratory under Contract No. W-7405-ENG-48.

[1] J. Lindl, Phys. Plasmas **V2**, 3933 (1995).
[2] E. M. Campbell and J. C. Browne, Science **271**, 130 (1996).
[3] A. J. Martin, R. J. Simms, and R. B. Jacobs, J. Vac. Sci. Technol. A **6**, 1885 (1988).
[4] J. K. Hoffer and L. R. Foreman, Phys. Rev. Lett. **60**, 1310 (1988).
[5] T. P. Bernat, E. R. Mapoles, and J. J. Sanchez, Lawrence Livermore National Laboratory, Report # UCRL-LR-105821-91-2, Inertial Confinement Fusion Quarterly Report, Vol. 1, pp. 57–61.
[6] C. Godrèche, *Solids Far From Equilibrium* (Cambridge University Press, Cambridge, 1992).
[7] C. Herring, *The Physics of Powder Metallurgy* (McGraw-Hill, New York, 1951), Chap. 8.
[8] C. Herring, *Structure and Properties of Solid Surfaces* (University of Chicago Press, Chicago, 1953).
[9] W. W. Mullins, J. Appl. Phys. **28**, 333 (1957).
[10] W. K. Burton, N. Cabrera, and F. C. Frank, Philos. Trans. R Soc. London, Series A **243**, 299 (1951).
[11] *Collected Papers of L. D. Landau*, edited by O. Ter Haar (Gordon and Breach, New York, 1965).
[12] B. J. Kozioziemski, G. W. Collins, and T. P. Bernat, Fusion Technol. **31**, 482 (1997).